with individual atoms. In certain other semiconductors, such as doped nickel oxide (Chapters 6, 7), the band model appears not to be suitable since these materials are best regarded as hopping semiconductors in which the electrons do not have high mobility. Instead, it appears to be more appropriate to regard the *d* electrons as occupying discrete orbitals on the nickel ions. It is important to remember, however, that the question of conduction in nickel oxide refers to only one or two sets of energy levels. NiO, like all materials, has many sets of energy levels. The lower lying levels are full and are discrete levels associated with the individual anions and cations. At higher energy various excited levels are usually completely empty but may overlap to form energy bands. In asking whether or not a bond or band model is the most suitable, one has to be clear about the particular property or set of energy levels to which the question refers. Thus many ionically bonded solids may, under UV irradiation, show electronic conductivity that is best described in terms of band theory.

Chapter 3

Crystallography and Diffraction Techniques

3.1 General comments: molecular and non-molecular solids

The simplest and most obvious first question to ask about an inorganic substance is 'What is it?'. The methods that are used to answer this come into two main categories, depending on whether the substance is molecular or non-molecular. If the substance is molecular, whether it be solid, liquid or gaseous, identification is usually carried out by some combination of spectroscopic methods and chemical analysis. If the substance is non-molecular and crystalline, identification is usually carried out by X-ray powder diffraction supplemented, where necessary, by chemical analysis. Each crystalline solid has its own characteristic X-ray powder pattern which may be used as a 'fingerprint' for its identification. The powder patterns of most known inorganic solids are included in an updated version of the *Powder Diffraction File* (Section 3.3e); by using an appropriate search procedure, unknowns can usually be identified rapidly and unambiguously.

Once the substance has been identified, the next stage may be to determine its structure, if this is not known already. For molecular materials, details of the molecular geometry may be obtained from further spectroscopic measurements. Alternatively, if the substance is crystalline, X-ray crystallography may be used, in which case information is also obtained on the way in which the molecules pack together in the crystalline state. For molecular substances, this usually completes the story as far as identification and structure determination are concerned; attention may then focus on other matters such as properties or chemical reactivity.

For non-molecular substances, however, the word 'structure' takes on a whole new meaning. Obviously, we need to know the *crystal structure*, as given by the unit cell and its contents. However, defects and impurities are also often extremely important and sometimes control properties. Thus, the colour and lasing action of ruby, Cr-doped Al_2O_3, depend exclusively on the presence of Cr^{3+} impurities in the corundum crystal structure of Al_2O_3. In such cases, the crystal structure or *average structure* of the host is important but the *local structure* centred on the impurities or defects controls the properties.

On a somewhat larger length scale, the optical properties of colloids (or nanoparticles, to give them a name that is currently more fashionable) depend

on crystallite size. For instance, the colour, band gap and photoconductivity of CdS nanoparticles depend on the particle size and hence, on their *nanostructure*.

On a still larger scale, the mechanical and electrical properties of ceramics are often determined by the *microstructure*, which covers the size, shape and distribution of crystalline grains, the bonding between grains and the segregation of any impurities to the surfaces or intergranular regions. To give one example, ZnO ceramic varistors are rather special materials whose electrical properties do not obey Ohm's Law and this is associated with compositional inhomogeneities in the ceramic, in particular the segregation of dopants such as Bi and Co to the intergranular regions.

When we refer to the structure of inorganic materials, we may be interested in some or all of the above aspects of structure, ranging from local structure, over distances of a few angstroms (1 Å = 0.1 nm = $10^{-4}\mu$m = 10^{-7} mm), to microstructure at the micron level. This contrasts hugely with molecular substances for which structure refers mainly to the atomic-level arrangement of atoms and occasionally, to the packing arrangement of molecules in crystals. Since in non-molecular materials we are interested in the structure at several levels, a wide range of techniques is needed to *characterize* the solids.

The prime reason for the great difference between molecular and non-molecular materials lies in the very different status of defects and impurities in the two categories of material. In molecular substances, defects are not allowed! If a certain molecule has atoms missing, or extra atoms present, then the resulting molecule is quite different to the parent molecule and can be separated by standard purification methods. Further, the presence of any such 'defective' molecules is most unlikely to modify the properties of the parent, non-defective molecules. Thus, molecules have accurately fixed formulae or stoichiometries and are defect-free.

In non-molecular materials by contrast, defects and impurities are almost unavoidable. They cannot be readily eliminated and are always present from thermodynamic considerations. Impurities give rise to *non-stoichiometry*, i.e. variable composition and may induce dramatic changes in properties of the parent structure.

An illustration of the vastly different chemistries of molecular and non-molecular substances is given in Table 3.1 for two apparently simple substances, one in each category. Molecular chemists will tell you that toluene is an extremely well-understood molecule and has few surprises left. Aluminium oxide, by contrast, shows a rich diversity of structures, properties and applications and is still being actively researched.

3.2 Characterization of solids

In order for a solid to be well characterized, one needs to know about:

(a) the crystal structure, as given by the unit cell, its dimensions and the fractional coordinates of the atoms present in the cell;
(b) the crystal defects that are present, their nature, number and distribution;

Table 3.1 *Comparison of a molecular substance, toluene, $C_6H_5CH_3$, and a non-molecular substance, Al_2O_3*

	Toluene	Alumina
Stoichiometry	Fixed, $C_6H_5CH_3$	Fixed, Al_2O_3
Impurities?	Not allowed	Readily doped
Nature of the material	Volatile liquid	Can be: powder, fibre, ceramic, single crystal, film
Properties		Depend on the nature of the material and dopants/impurities
Applications	Solvent	Abrasive (powder), thermal insulator (saffil fibres), electrical insulator (thin film or ceramic substrate), ruby gem and laser (Cr doped), solid electrolyte (Na beta-alumina)

(c) the impurities that are present and whether they are distributed at random or are concentrated into small regions;
(d) for polycrystalline solids—powders or ceramics—the number, size, shape and distribution of the crystalline particles;
(e) the surface structure, including any compositional inhomogeneities, absorbed surface layers or structural differences between surface and interior.

No single technique is capable of providing a complete characterization of a solid. Rather, a variety of techniques are used in combination. There are three main categories of physical technique which may be used to characterize solids: diffraction, microscopic and spectroscopic techniques. In addition, other techniques such as thermal analysis and physical property measurements give valuable information in certain cases. This chapter deals with diffraction techniques; several of the other techniques are considered in Chapter 4.

X-ray diffraction has been used for nearly a century in two main areas, for the fingerprint characterization of crystalline materials and for determination of their structure. It is the principal technique of solid state chemistry and accordingly, is given most space in this chapter. A brief description is also given of electron and neutron diffraction, two rather specialized techniques which have important applications.

3.3 X-ray diffraction

a) Generation of X-rays

X-rays are electromagnetic radiation of wavelength ~ 1 Å (10^{-10}m). They occur in that part of the electromagnetic spectrum between γ-rays and the ultraviolet. X-rays are produced when high-energy charged particles, e.g. electrons accelerated through 30,000 V, collide with matter. The resulting X-ray spectra usually have two components, a broad spectrum of wavelengths known as *white radiation* and a number of fixed, or monochromatic wavelengths.

White radiation arises when the electrons are slowed down or stopped by the collision and some of their lost energy is converted into electromagnetic radiation. White radiation has wavelengths ranging upwards from a certain lower limiting value. This lower wavelength limit corresponds to the X-rays of highest energy and occurs when all the kinetic energy of the incident particles is converted into X-rays. It may be calculated from the formula, $\lambda_{min}(\text{Å}) = 12400/V$, where V is the accelerating voltage.

The X-rays which are used in almost all diffraction experiments are produced by a different process that leads to *monochromatic X-rays*. A beam of electrons, again accelerated through, say, 30 kV is allowed to strike a metal *target*, often Cu. The incident electrons have sufficient energy to ionize some of the Cu 1*s* (*K* shell) electrons, Fig. 3.1(a). An electron in an outer orbital (2*p* or 3*p*) immediately drops down to occupy the vacant 1*s* level and the energy released in the transition appears as X-radiation. The transition energies have fixed values and so a spectrum of characteristic X-rays results, Fig. 3.1(b). For Cu the $2p \rightarrow 1s$ transition, called $K\alpha$, has a wavelength of 1.5418 Å and the $3p \rightarrow 1s$ transition, $K\beta$, 1.3922 Å. The $K\alpha$ transition occurs much more frequently than the $K\beta$ transition and this more intense $K\alpha$ radiation is used in diffraction experiments. In fact, the $K\alpha$ transition is a doublet, $K\alpha_1 = 1.54051$ Å and $K\alpha_2 = 1.54433$ Å, because the transition has a slightly different energy for the two possible spin states of the 2*p* electron which makes the transition, relative to the spin of the vacant 1*s* orbital. In some X-ray experiments, diffraction by the $K\alpha_1$ and $K\alpha_2$ radiations is not resolved and a single line or spot is observed instead of a doublet (e.g. in powder diffractometry at low angle). In other experiments, separate diffraction peaks may be observed; if desired, this can be overcome by removing the weaker $K\alpha_2$ beam from the incident radiation.

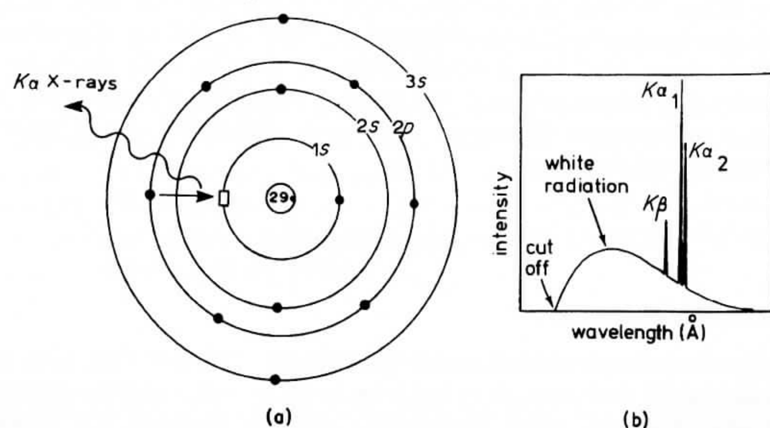

Fig. 3.1 (a) Generation of Cu $K\alpha$ X-rays. A 1*s* electron is ionized; a 2*p* electron falls into the empty 1*s* level (□) and the excess energy is released as X-rays. (b) X-ray emission spectrum of Cu

Table 3.2 *X-ray wavelengths (Å) of commonly used target materials*

Target	$K\alpha_1$	$K\alpha_2$	$K\bar{\alpha}$*	Filter
Cr	2.2896	2.2935	2.2909	V
Fe	1.9360	1.9399	1.9373	Mn
Cu	1.5405	1.5443	1.5418	Ni
Mo	0.7093	0.7135	0.7107	Nb
Ag	0.5594	0.5638	0.5608	Pd

* $\bar{\alpha}$ is the intensity-weighted average of α_1 and α_2.

The wavelengths of the $K\alpha$ lines of the target metals commonly used for X-ray generation are given in Table 3.2. They are related to the atomic number Z, of the metal, by *Moseley's law*:

$$\lambda^{-1/2} = C(Z - \sigma) \qquad (3.1)$$

where C and σ are constants. Hence the wavelength of the $K\alpha$ line decreases with increasing atomic number.

The X-ray emission spectrum of an element such as Cu, Fig. 3.1(b), has two main features. The intense, monochromatic peaks, caused by electronic transitions within the atoms, have wavelengths that are characteristic of the element, i.e. Cu. These peaks are superposed on a background of white radiation produced by the general interaction of high-velocity electrons with matter. In order to generate the characteristic monochromatic radiation, the voltage used to accelerate the electrons needs to be sufficiently high (≥ 10 kV) that ionization of the Cu 1*s* electrons occurs.

In the generation of X-rays, Fig. 3.2, the electron beam, provided by a heated tungsten filament, is accelerated towards an anode by a potential difference of ~ 30 kV. The electrons strike the target, a piece of Cu fixed to the anode, and a spectrum of X-rays, such as shown in Fig. 3.1(b), is emitted. The chamber, known as the *X-ray tube*, is evacuated to prevent oxidation of the W filament. The X-rays leave the tube through 'windows' made of Be. The absorption of X-rays on passing through materials depends on the atomic weight of the elements

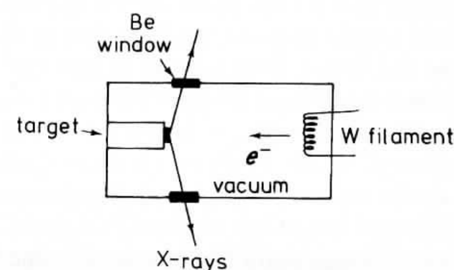

Fig. 3.2 Schematic design of a filament X-ray tube

present. Be with an atomic number of 4 is, therefore, one of the most suitable window materials. For the same reason, lead is a very effective material for shielding X-ray equipment and absorbing stray radiation. While an X-ray tube is in operation, continuous cooling of the anode is necessary. Only a small fraction of the energy of the incident electron beam is converted into X-rays. Most of the energy is converted into heat and the anode would soon melt if it were not cooled.

For most diffraction experiments, a monochromatic beam of X-rays is desired and not a continuous spectrum. In the spectrum of X-rays emitted by Cu (or any metal), the $K\alpha$ line(s) is the most intense and it is desired to filter out all other wavelengths, leaving the $K\alpha$ line for diffraction experiments. For Cu radiation, a sheet of Ni foil is a very effective filter. The energy required to ionize $1s$ electrons of Ni corresponds to a wavelength of 1.488 Å, which lies between the values for the $K\alpha$ and $K\beta$ lines of the Cu emission spectrum. Cu $K\beta$ radiation, therefore, has sufficient energy to ionize $1s$ electrons of Ni whereas Cu $K\alpha$ radiation does not. Ni foil is effective in absorbing the Cu $K\beta$ radiation and most of the white radiation, leaving a monochromatic, reasonably clean beam of $K\alpha$ radiation. A lighter element, such as Fe, would absorb Cu $K\alpha$ radiation as well as $K\beta$, because its *absorption edge* is displaced to higher wavelengths. On the other hand, a heavier element, such as Zn, would transmit both $K\alpha$ and $K\beta$ radiations while still absorbing much of the higher-energy white radiation. The atomic number of the element in the filter generally is one or two less than that of the target material, Table 3.2. An alternative method of obtaining monochromatic X-rays uses a single crystal monochromator and is discussed later.

b) An optical grating and diffraction of light

As an aid to understanding the diffraction of X-rays by crystals, let us consider the diffraction of light by an optical grating. This gives a one-dimensional (1D) analogue of the 3D process that occurs in crystals. An optical grating is a piece of glass on which have been ruled a large number of accurately parallel and closely spaced lines. The separation of the lines is a little larger than the wavelength of light, say 10,000 Å. The grating is shown in projection as a row of points in Fig. 3.3(a). Consider what happens to a beam of light which hits the grating perpendicular to the plane of the grating. A piece of glass without the lines would simply transmit the light, but in the grating the lines act as secondary point (or, rather, line) sources of light and re-radiate light in all directions. Interference then occurs between the waves originating from each line source. In certain directions, adjacent beams are in phase with each other and *constructive interference* occurs to give a resultant diffracted beam in that direction. Two such directions are shown in (b). In direction 1, parallel to the incident beam, the diffracted beams are obviously in phase. In direction 2, the beams are also in phase although beam B is now exactly one wavelength behind beam A. For directions between 1 and 2, B lags A by a fraction of one wavelength, and *destructive interference* occurs. For a certain direction, 3, B is

exactly half a wavelength behind A and complete destructive interference or *cancellation* occurs. For other directions between 1 and 2, the destructive interference is only partial. Thus, directions 1 and 2 have maximum light intensity and this falls off gradually to zero as the angle changes to direction 3. In the optical grating, however, there are not just two parallel diffracted beams A and B but several hundred or thousand, one for each line on the grating. This causes the resultant diffracted beams to sharpen enormously after interference so that intense beams occur in directions 1 and 2 with virtually no intensity over the whole range of directions between 1 and 2.

The directions, such as 2, in which constructive interference occurs are governed by the wavelength of the light, λ, and the separation, a, of the lines on the grating. Consider the diffracted beams 1 and 2, Fig. 3.4, which are at an angle, ϕ, to the direction of the incident beam. If 1 and 2 are in phase, the distance AB must equal a whole number of wavelengths; i.e.

$$AB = \lambda, 2\lambda, \ldots, n\lambda$$

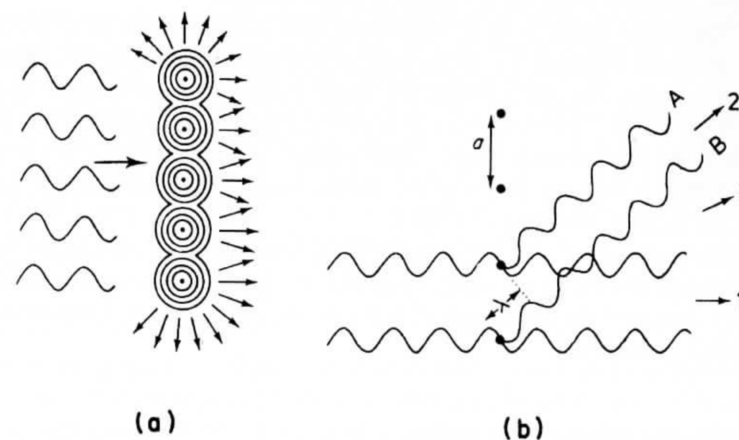

Fig. 3.3 (a) Lines on an optical grating act as secondary sources of light. (b) Constructive interference in directions 1 and 2

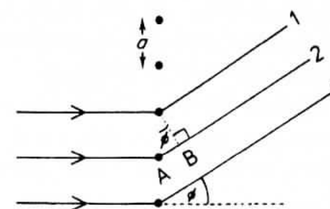

Fig. 3.4 Diffraction of light by an optical grating

But

$$AB = a \sin\phi$$

Therefore,

$$a \sin \phi = n\lambda \tag{3.2}$$

This equation gives the conditions under which constructive interference occurs and relates the spacing of the grating to the light wavelength and the diffraction order, n. Hence, depending on the value of $a \sin \phi$, one or more diffraction orders, corresponding to $n = 1, 2$, etc., may be observed.

We can now understand why the separation of lines on the grating must be of the same order of magnitude as, but somewhat larger than, the wavelength of light. The condition for the first-order diffracted beam to occur is $a \sin \phi = \lambda$. The maximum value of $\sin \phi$ is 1, corresponding to $\phi = 90°$ but realistically, in order to observe first-order diffraction, $\sin \phi < 1$ and, therefore, $a > \lambda$. If $a < \lambda$, only the zero order direct beam is observable.

If, on the other hand, $a \gg \lambda$, individual diffraction orders ($n = 1, 2, 3, \ldots$, etc.) are so close together as to be unresolved and, effectively, a diffraction continuum results. This is because, for large values of a, $\sin \phi$ and, hence, ϕ must be very small. Therefore $\phi_{n=1} \geq 0$ and the first-order beam is not distinguishable from the primary beam. Visible light has wavelengths in the range 4,000 to 7,000 Å and so, in order to observe well-separated spectra, grating spacings are usually 10,000 to 20,000 Å.

The other condition to be observed in the construction of an optical grating is that the lines should be accurately parallel. If this were not so, ϕ would vary over the grating and the diffraction spectra would be blurred or irregular and of poor quality generally.

c) Crystals and diffraction of X-rays

By analogy with the diffraction of light by an optical grating, crystals, with their regularly repeating structures, should be capable of diffracting radiation that has a wavelength similar to interatomic separations, ~ 2–3 Å. Three types of radiation are used for crystal diffraction studies: X-rays, electrons and neutrons. Of these, X-rays are the most useful but electron and neutron diffraction also have important specific applications and are discussed later. The X-ray wavelength commonly employed is the characteristic $K\alpha$ radiation, $\lambda = 1.5418$ Å, emitted by Cu. When crystals diffract X-rays, the atoms or ions act as secondary point sources and scatter the X-rays; in the optical grating, the lines scratched or ruled on the glass surface cause scattering.

Historically, two approaches have been used to treat diffraction by crystals. These are as follows.

i) *The Laue equations*

Diffraction from a hypothetical 1D crystal, constituting a row of atoms, may be treated in the same way as diffraction of light by an optical grating because, in projection, the grating is a row of points. An equation is obtained which relates the separation, a, of the atoms in the row, the X-ray wavelength, λ, and the diffraction angle, ϕ; i.e.

$$a \sin\phi = n\lambda$$

A real crystal is a 3D arrangement of atoms for which three *Laue equations* may be written:

$$a_1 \sin\phi_1 = n\lambda$$

$$a_2 \sin\phi_2 = n\lambda$$

$$a_3 \sin\phi_3 = n\lambda$$

The equations correspond to each of the three crystallographic axes needed to represent the atomic arrangement in the crystal. For a diffracted beam to occur, these three equations must be satisfied simultaneously.

The Laue equations provide a rigorous and mathematically correct way to describe diffraction by crystals. The drawback is that they are cumbersome to use. The alternative theory of diffraction, based on Bragg's law, is much simpler and is used almost universally in solid state chemistry. No further discussion of the Laue equations is given in this book.

ii) *Bragg's law*

The Bragg approach to diffraction is to regard crystals as built up in layers or planes such that each acts as a semi-transparent mirror. Some of the X-rays are reflected off a plane with the angle of reflection equal to the angle of incidence, but the rest are transmitted to be subsequently reflected by succeeding planes.

The derivation of Bragg's law is shown in Fig. 3.5. Two X- ray beams, 1 and 2, are reflected from adjacent planes, A and B, within the crystal and we wish to know under what conditions the reflected beams 1′ and 2′ are in phase. Beam 22′ has to travel the extra distance xyz as compared to beam 11′, and for 1′ and 2′ to be in phase, distance xyz must equal a whole number of wavelengths. The perpendicular distance between pairs of adjacent planes, the *d-spacing*, d, and the angle of incidence, or *Bragg angle*, θ, are related to the distance xy by

$$xy = yz = d \sin\theta$$

Thus

$$xyz = 2d \sin\theta$$

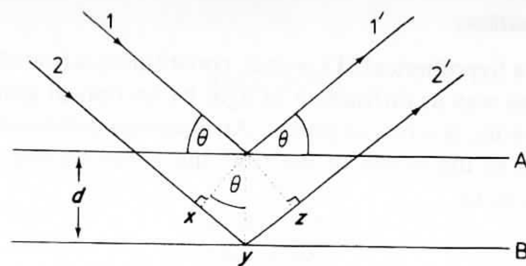

Fig. 3.5 Derivation of Bragg's law

But

$$xyz = n\lambda$$

Therefore

$$2d\sin\theta = n\lambda \quad \textit{Bragg's law} \tag{3.3}$$

When Bragg's law is satisfied, the reflected beams are in phase and interfere constructively. At angles of incidence other than the Bragg angle, reflected beams are out of phase and destructive interference or cancellation occurs. In real crystals, which contain thousands of planes and not just the two shown in Fig. 3.5, Bragg's law imposes a stringent condition on the angles at which reflection may occur. If the incident angle is incorrect by more than a few tenths of a degree, cancellation of the reflected beams is usually complete.

For a given set of planes, several solutions of Bragg's law are usually possible, for $n = 1, 2, 3$, etc. It is customary, however, to set n equal to 1 and for situations where, say, $n = 2$, the d-spacing is instead halved by doubling up the number of planes in the set; hence n is kept equal to 1. (Note that $2\lambda = 2d\sin\theta$ is equivalent to $\lambda = 2(d/2)\sin\theta$.)

It is difficult to give an explanation of the nature of the semi-transparent layers or planes that is immediately convincing. This is because they are a concept rather than a physical reality. Crystal structures, with their regularly repeating patterns, may be referred to a 3D grid and the repeating unit of the grid, the *unit cell*, can be found. The grid may be divided up into sets of planes in various orientations and it is these planes which are considered in the derivation of Bragg's law. In some cases, with simple crystal structures, the planes also correspond to layers of atoms, but this is not generally the case.

Some of the assumptions upon which Bragg's law is based may seem to be rather dubious. For instance, it is known that diffraction occurs as a result of interaction between X-rays and atoms. Further, the atoms do not *reflect* X-rays but scatter or diffract them in all directions. Nevertheless, the highly simplified treatment that is used in deriving Bragg's law gives exactly the same answers as are obtained by a rigorous mathematical treatment. We therefore happily use

terms such as reflexion (often deliberately with this alternative spelling) and bear in mind that we are fortunate to have such a simple and picturesque, albeit inaccurate, way to describe what in reality is a very complicated process.

d) X-ray diffraction methods

When reduced to basic essentials, the X-ray diffraction experiment, Fig. 3.6, requires an X-ray source, the sample under investigation and a detector to pick up the diffracted X-rays. Within this broad framework, three variables govern the different X-ray techniques:

(a) radiation—monochromatic or of variable λ;
(b) sample—single crystal, powder or a solid piece;
(c) detector—radiation counter or photographic film.

These are summarized for the most important techniques in Fig. 3.7. With the exception of the Laue method, which is used almost exclusively by metallurgists and is not discussed here, monochromatic radiation is nearly always used.

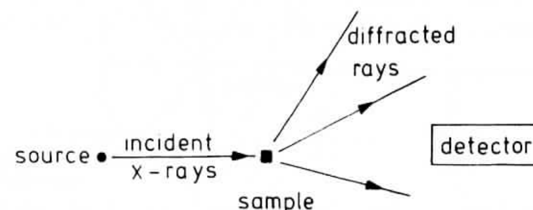

Fig. 3.6 The X-ray diffraction experiment

WAVELENGTH	*SAMPLE*	*DETECTOR*	*METHOD*
Fixed	Powder	Counter	Diffractometer
		Film	Debye-Scherrer Guinier (Focusing)
	Single crystal	Film	Rotation (Oscillation) Weissenberg Precession (Buerger)
		Counter	Automatic Diffractometer
Variable	Solid piece	Film	Laue

Fig. 3.7 The different X-ray diffraction techniques

e) The powder method—principles and uses

The principles of the powder method are shown in Fig. 3.8. A monochromatic beam of X-rays strikes a finely powdered sample that, ideally, has crystals randomly arranged in every possible orientation. In such a powder sample, the various lattice planes are also present in every possible orientation. For each set of planes, therefore, at least some crystals must be oriented at the Bragg angle, θ, to the incident beam and thus, diffraction occurs for these crystals and planes. The diffracted beams may be detected either by surrounding the sample with a strip of photographic film (Debye–Scherrer and Guinier focusing methods) or by using a movable detector, such as a Geiger counter or scintillation counter, connected to a chart recorder or computer (diffractometer).

The original powder method, the *Debye–Scherrer method,* is little used nowadays, but since it is simple it is instructive to consider its mode of operation. For any set of lattice planes, the diffracted radiation forms the surface of a cone, as shown in Fig. 3.9. The only requirement for diffraction is that the planes be at angle θ to the incident beam; no restriction is placed on the angular orientation of the planes about the axis of the incident beam. In a finely powdered sample, crystals are present at every possible angular position about the incident beam and the diffracted beams that result appear to be emitted from the sample as cones of radiation (each cone is in fact a large number of closely spaced diffracted beams). If the Bragg angle is θ, then the angle between diffracted and undiffracted beams is 2θ and the angle of the cone is 4θ. Each set of planes gives its own cone of radiation. The cones are detected by a thin strip of film wrapped around the sample, Fig. 3.8; each cone intersects the film as two short arcs, Fig. 3.10, which are symmetrical about the two holes in the film (these allow entry and exit of incident and undiffracted beams). In a well-powdered sample, each arc appears as a continuous line, but in coarser samples the arcs may be spotty due to the relatively small number of crystals present.

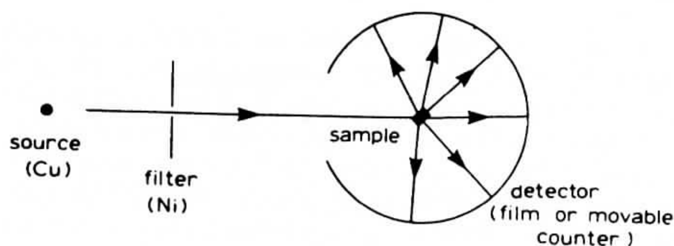

Fig. 3.8 The powder method

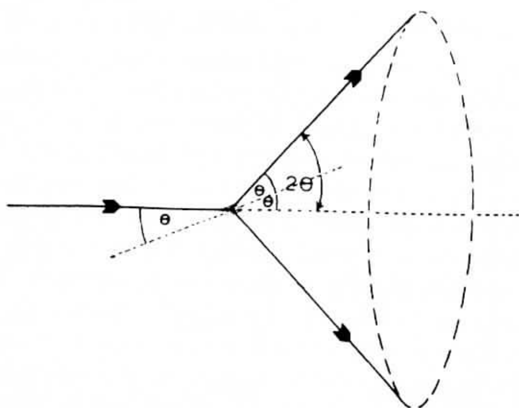

Fig. 3.9 Formation of a cone of diffracted radiation

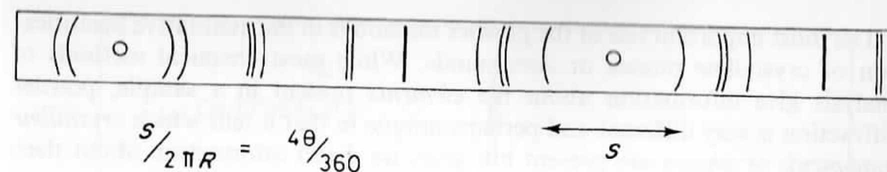

Fig. 3.10 Schematic Debye–Scherrer photograph

To obtain *d*-spacings from the Debye–Scherrer film, the separation, S, between pairs of corresponding arcs is measured. If the camera (film) radius, R, is known, then

$$\frac{S}{2\pi R} = \frac{4\theta}{360} \tag{3.4}$$

from which 2θ and therefore d may be obtained for each pair of arcs. The disadvantages of this method are that exposure times are long (6 to 24 hours) and that closely spaced arcs are not well resolved. This is because, although the incident beam enters the camera through a pinhole slit and collimator tube, the beam is somewhat divergent and the spread increases in the diffracted beams. If, in an effort to increase the resolution, a finer collimator is used, the resulting diffracted beams have much less intensity and longer exposure times are needed. Apart from considerations of the extra time involved, the amount of background radiation detected by the film (as fogging) increases with exposure time and, consequently, weak lines may be lost altogether in the background.

In modern film methods (*Guinier focusing methods*) a *convergent*, intense incident beam is used with the result that excellent resolution of lines is obtained and exposure times are much reduced (10 min to 1 hr). Methods for obtaining a convergent beam of X-rays are discussed in the next section.

The other modern powder technique is *diffractometry*, which gives a series of peaks on a strip of chart paper or on a PC screen. A convergent incident beam is again used to give fairly good resolution of peaks. Both peak positions and intensities (peak heights) are readily obtained from the chart to make this a very useful and rapid method of phase analysis.

The most important use of the powder method is in the qualitative identification of crystalline phases or compounds. While most chemical methods of analysis give information about the *elements* present in a sample, powder diffraction is very different and perhaps unique in that it tells which *crystalline compounds* or *phases* are present but gives no direct information about their chemical constitution.

Each crystalline phase has a characteristic powder pattern which can be used as a fingerprint for identification purposes. The two variables in a powder pattern are peak position, i.e. d-spacing, which can be measured very accurately if necessary, and intensity, which can be measured either qualitatively or quantitatively. It is rare but not unknown that two materials have identical powder patterns. More often, two materials have one or two lines with common d-spacings, but on comparing the whole patterns, which may contain between ~ 5 and > 100 observed lines, the two are found to be quite different. The normal practice in using powder patterns for identification purposes is to pay most attention to the d-spacings but, at the same time, check that the intensities are roughly correct.

For the identification of unknown crystalline materials, an invaluable reference source is the *Powder Diffraction File* (International Centre for Diffraction Data, USA), previously known as the ASTM or JCPDS file, which contains the powder patterns of about 35,000 materials; new entries are added at the current rate of $\sim$ 2,000 p.a. In the search indices, materials are classified either according to their most intense peaks or according to the first eight lines in the powder pattern in order of decreasing d-spacing. Identification of an unknown is usually possible within 30 min of obtaining its measured powder pattern. Problems arise if the material is not included in the file (obviously!) or if the material is not pure but contains lines from more than one phase.

f) Powder diffractometers

The powder diffractometer has a proportional, scintillation or Geiger counter which scans a range of 2θ values at constant angular velocity (it is common practice to refer to the angle 2θ between diffracted and undiffracted beams, Fig. 3.9, rather than to the Bragg angle, θ). Usually, the range 10 to 80° 2θ is sufficient to cover the most useful part of the powder pattern. A typical diffractometer trace is shown in Fig. 3.11(a) for SiO_2. The scale is linear in 2θ and d-spacings of the peaks may be calculated from Bragg's law or obtained from standard tables of d versus 2θ. The scanning speed of the counter is usually $2° \ 2\theta \ \text{min}^{-1}$ and, therefore, about 30 min are needed to obtain a trace. Intensities are taken as either peak heights or for accurate work peak areas; the most intense peak is given an intensity of 100 and the rest are scaled accordingly. For accurate d-spacings, an internal standard (a pure material, such as KCl, whose d-spacings are known accurately) is mixed in with the sample. A correction factor, which may vary with 2θ, is obtained from the discrepancy between observed and true d-spacings of the standard and is then applied to the pattern that is being measured.

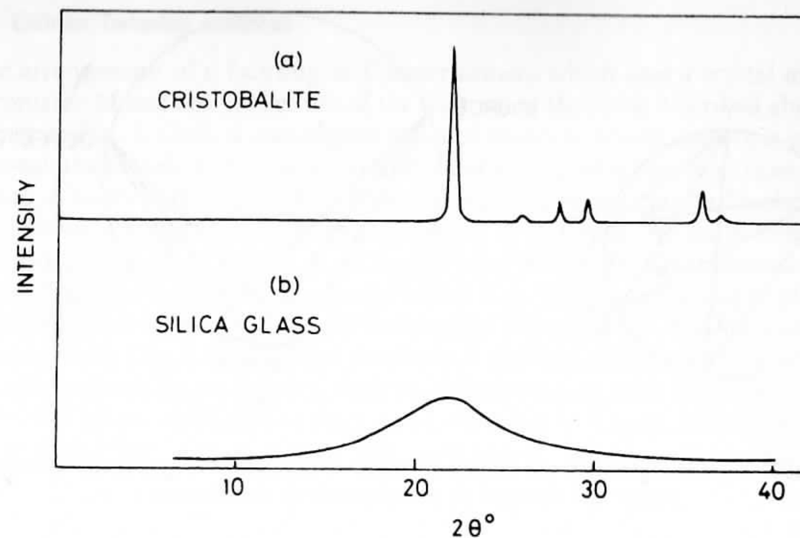

Fig. 3.11 X-ray powder diffraction pattern of (a) cristobalite and (b) glassy SiO_2, Cu$K\alpha$ radiation

Samples for diffractometry take various forms: they include thin layers of fine powder sprinkled onto a glass slide smeared with vaseline and thin flakes pressed onto a glass slide. The objective is always to obtain a sample which contains a random arrangement of crystal orientations. If the crystal arrangement is not random, then *preferred orientation* exists and can introduce errors, sometimes very large, into the measured intensities. Preferred orientation is a serious problem for materials that crystallize in a characteristic, very non-spherical shape, e.g. clay minerals which usually occur as thin plates or some cubic materials which crystallize as cubes and, on crushing, break up into smaller cubes. In a powder aggregate of such materials, the crystals tend to sit on their faces, resulting in a non-random average orientation.

g) Focusing of X-rays: theorem of a circle

A big disadvantage of Debye–Scherrer cameras is that incident and diffracted beams are, inevitably, divergent and of low intensity. In diffractometers and modern focusing cameras, a convergent X-ray beam is used; this gives a dramatic improvement in resolution and, because much more intense beams may be used, exposure times are greatly reduced. It is not possible to focus or converge X-rays using the X-ray equivalent of an optical lens; instead, use is made of certain geometric properties of the circle in order to obtain a convergent X-ray beam. These properties are illustrated in Fig. 3.12(a). The arc XY forms part of a circle and all angles subtended on the circumference of this circle by the arc XY are equal, i.e. $XCY = XC'Y = XC''Y = \alpha$. Suppose that X

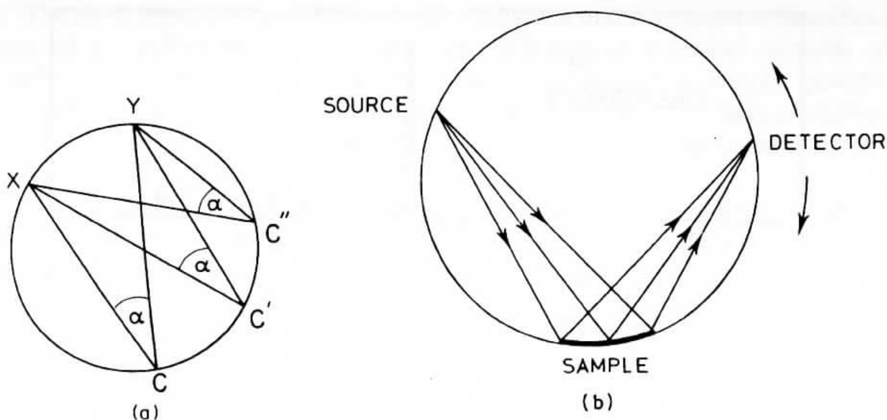

Fig. 3.12 (a) Theorem of a circle used to focus X-rays. (b) Arrangement of sample, source and detector on the circumference of a circle

is a source of X-rays and XC, XC′ represent the extremities of a divergent X-ray beam emitted from X. If the beam is diffracted by a sample which covers the arc between C and C′ such that the diffracting planes are tangential to the circle, then the diffracted beam, represented by CY and C′Y, will focus to a point at Y. The principle of the focusing method is therefore to arrange that the source of X-rays, the sample and the detector all lie on the circumference of an appropriate circle.

h) Crystal monochromators

The same focusing principle is used in the construction of diffractometers and focusing cameras, although several different arrangements are found in commercial instruments. An additional feature is often the inclusion of a *crystal monochromator* which serves two functions: to give highly monochromatic radiation and to produce an intense, convergent X-ray beam. There are several sources of background scattering in diffraction experiments, one of which is radiation of wavelength different from that of the $K\alpha$ radiation. $K\alpha$ radiation may be separated from the rest by the use of filters or, better, by a crystal monochromator.

A crystal monochromator consists of a large single crystal of, for example, quartz, oriented such that one set of planes which diffracts strongly ($10\bar{1}1$ for quartz) is at the Bragg angle to the incident beam. This Bragg angle is calculated for $\lambda_{k\alpha_1}$ and so only the $K\alpha_1$ rays are diffracted, giving monochromatic radiation. If a flat crystal monochromator were used, much of the $K\alpha_1$ radiation would be lost since the X-ray beam emitted from a source is naturally divergent; only a small amount of the $K\alpha_1$ component would therefore be at the correct Bragg angle to the monochromator. To improve the efficiency, the crystal monochromator is bent, in which case a divergent X-ray beam may be used which is diffracted by the crystal monochromator to give a beam that is intense, monochromatic and convergent.

i) Guinier focusing cameras

The arrangement of a focusing or Guinier camera which uses a crystal monochromator M and also makes use of the theorem of the circle described above is shown in Fig. 3.13(a). A convergent beam of monochromatic radiation passes through the sample at X. Radiation that is not diffracted comes to a focus at A, where a beam stop is placed in front of the film to prevent its blackening. Various beams diffracted by the sample focus at B, C, etc. We know from the theorem of the circle that A, B, C and X must lie on the circumference of a circle. The film is placed in a cassette which is in the form of a short cylinder and lies on the circle ABC. The scale of the film is linear in 2θ. A schematic film is as shown in Fig. 3.13(b) except that instead of peaks of different height, lines of different intensity or different degrees of blackness are seen. Film dimensions are $\sim 1 \times 15$ cm which makes them very convenient to handle. The line at $0°2\theta$ or ∞ d-spacing corresponds to the undiffracted beam at A in (a). This

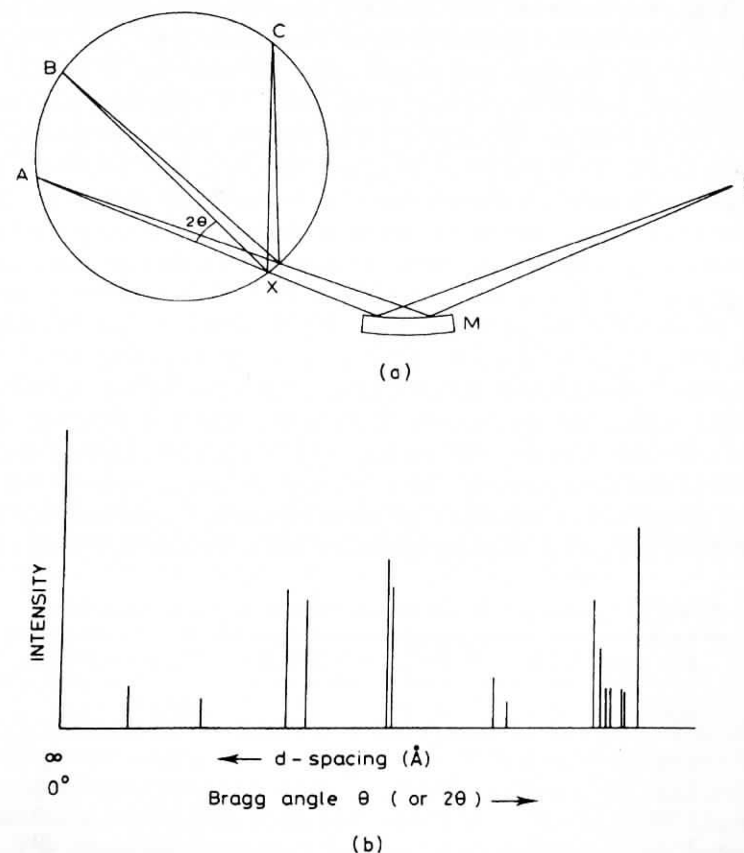

Fig. 3.13 (a) Crystal monochromator M, source S and sample X, in a focusing camera. (b) Schematic Guinier X-ray powder diffraction pattern

is the reference position on the film. The mark is made by removing the beam stop for a fraction of a second while the X-rays are switched on. If required, a scale may be printed onto the film and the positions of the lines, relative to A, may be measured with a travelling microscope or, better, by microdensitometry; 2θ values and *d*-spacings may then be computed or obtained from tables.

The Guinier method is capable of giving accurate *d*-spacings with results comparable to those obtained by diffractometry. Intensities are either estimated visually or measured using microdensitometry. Sample sizes are small, $\lesssim 1$ mg, and exposure times vary between 5 min and 1 hr, depending on factors such as the crystallinity of the sample and the presence or absence of heavy elements which absorb X-rays.

j) A powder pattern of a crystalline phase is its 'fingerprint'

There are two main factors which determine powder patterns: (a) the size and shape of the unit cell and (b) the atomic number and position of the atoms in the cell. Thus, two materials may have the same crystal structure but almost certainly will have distinct powder patterns. For example, KF, KCl and KI all have the rock salt structure and should show the same set of lines in their powder patterns, but, as can be seen from Table 3.3, both the positions and intensities of the lines are different in each. The positions or *d*-spacings vary because the unit cells are of different size and, therefore, the *a* parameter in the *d*-spacing formula varies. Intensities differ because different anions with different atomic numbers and therefore different scattering powers are present in the three materials, even though the atomic coordinates are the same for each (i.e. cations at corner and face centre positions, etc.). KCl is a rather extreme example because the intensities of 111 and 311 reflections are too small to measure, but it serves to illustrate the importance of scattering power of the atoms present. Intensities are discussed in more detail in the next section.

A powder pattern has two characteristic features, therefore: the *d*-spacings of the lines and their intensity. Of the two, the *d*-spacing is more useful and capable of precise measurement. The *d*-spacings should be reproducible from sample to sample unless impurities are present to form a solid solution. Intensities are more difficult to measure quantitatively and often vary from sample

Table 3.3 *X-ray powder diffraction patterns for potassium halides*

	KF, $a = 5.347$ Å		KCl, $a = 6.2931$ Å		KI, $a = 7.0655$ Å	
(*hkl*)	*d*(Å)	*I*	*d*(Å)	*I*	*d*(Å)	*I*
111	3.087	29		—	4.08	42
200	2.671	100	3.146	100	3.53	100
220	1.890	63	2.224	59	2.498	70
311	1.612	10	—	—	2.131	29
222	1.542	17	1.816	23	2.039	27
400	1.337	8	1.573	8	1.767	15

to sample especially if preferred orientation is present. Thus, the differences in tabulated intensities for, say, the (220) reflection of the three materials in Table 3.3 are probably not absolute, quantitatively.

The likelihood of two materials having the small cell parameters and *d*-spacings decreases considerably with decreasing crystal symmetry. Thus, cubic materials have only one variable, *a*, and there is a fair chance of finding two materials with the same *a* value. On the other hand, triclinic powder patterns have six variables, a, b, c, α, β and γ, and so accidental coincidences are far less likely. Problems of identification, if they occur, are most likely to be experienced with high symmetry, especially cubic, materials or in cases where similar-sized ions may replace each other in a particular structure.

k) Intensities

Intensities of X-ray reflections are important for two main reasons. First, quantitative measurements of intensity are necessary in order to solve crystal structures. Second, qualitative or semi-quantitative intensity data are needed in using the powder fingerprint method to characterize materials and especially in using the *Powder Diffraction File* to identify unknowns. Although this book is not concerned with the methods of structure determination, it is important that the factors which control the intensity of X-ray reflections be understood. The topic falls into two parts: the intensity scattered by individual atoms and the resultant intensity scattered from the large number of atoms in a crystal.

i) Scattering of X-rays by an atom: atomic scattering factors

Atoms diffract or scatter X-rays because an incident X-ray beam, which can be described as an electromagnetic wave with an oscillating electric field, sets each electron of an atom into vibration. A vibrating charge such as an electron emits radiation which is in phase or *coherent with* the incident X-ray beam. The electrons therefore act as secondary point sources of X-rays. Coherent scattering may be likened to an elastic collision between the wave and the electron: the wave is deflected by the electron without loss of energy and, therefore, without change of wavelength. The intensity of the radiation scattered coherently by 'point source' electrons is given by the *Thomson equation*:

$$I_P \propto \frac{1}{2}(1 + \cos^2 2\theta) \qquad (3.5)$$

where I_P is the scattered intensity at any point, P, and 2θ is the angle between the directions of the incident beam and the diffracted beam that passes through P. From this equation, the scattered beams are most intense when parallel or antiparallel to the incident beam and are weakest when at 90° to the incident beam. The Thomson equation is also known as the *polarization factor* and is one of the standard angular correction factors that must be applied when processing intensity data for use in structure determination.

At this point, it is worth mentioning that X-rays can interact with electrons in a different way to give *Compton scattering*. Compton scattering is rather like an inelastic collision in that the X-rays lose some of their energy on impact and so the scattered X-rays are of longer wavelength than the incident X-rays. They are also no longer in phase with the incident X-rays; nor are they in phase with each other. Compton scattering is caused by interaction between X-rays and more loosely held valence electrons; it is an important effect with the lighter elements and can have a particularly deleterious effect on the powder patterns of organic materials such as polymers. A close similarity exists between Compton scattering and the generation of white radiation in an X-ray tube; both are examples of incoherent scattering that are sources of background radiation in X-ray diffraction experiments.

The X-rays scattered by an atom are the resultant of the waves scattered by each electron in the atom. Electrons may be regarded as particles that momentarily occupy different positions in an atom and interference occurs between their scattered waves. For scattering in the direction of the incident beam, Fig. 3.14(a), beams 1′ and 2′, all electrons scatter in phase irrespective of their position. The scattered intensity is, then, the sum of the individual intensities. The *scattering factor*, or *form factor*, f, of an atom is proportional to its atomic number, Z, or, more strictly, to the number of electrons possessed by that atom.

For scattering at some angle 2θ to the direction of the incident beam, a phase difference, corresponding to the distance XY, exists between beams 1″ and 2″. This phase difference is usually rather less than one wavelength (i.e. XY < 1.5418 Å for Cu $K\alpha$ X-rays) because distances between electrons within an atom are short. As a result, only partial destructive interference occurs between 1″ and 2″. The net effect of interference between the beams scattered by all the electrons in the atom is to cause a gradual decrease in scattered intensity with increasing angle, 2θ. For example, the scattering power of Cu is proportional to 29 (i.e. Z) at $2\theta = 0°$, to 14 at 90° and to 11.5 at 120°. It should also be apparent that for a given angle, 2θ, the net intensity decreases with decreasing X-ray wavelength because the phase difference XY gives a greater degree of cancellation for smaller λ. The form factors of atoms are given in *International Tables for X-ray Crystallography*, Vol. 3 (1952). They are tabulated against $(\sin\theta/\lambda)$ to include the effect of both angle and X-ray wavelength; examples are shown in Fig. 3.14(b).

Two consequences of the dependence of form factors on $\sin\theta/\lambda$ and atomic number are as follows. First, powder patterns at high angles (above ~ 60 to 70° 2θ) are usually weak. Second, in X-ray crystal structure determination it is difficult to locate light atoms because their diffracted radiation is so weak. Thus H cannot usually be located unless all the other elements present are also extremely light. Atoms that have as many electrons as oxygen can usually be located easily unless a very heavy atom such as uranium is present. Structures that are particularly difficult to solve are those in which a considerable number or all of the atoms have similar atomic number, e.g. large organic molecules with C, N and O. In such cases, a common ploy is to make a derivative of the compound of interest which contains a heavy metal atom. The heavy atoms are detected

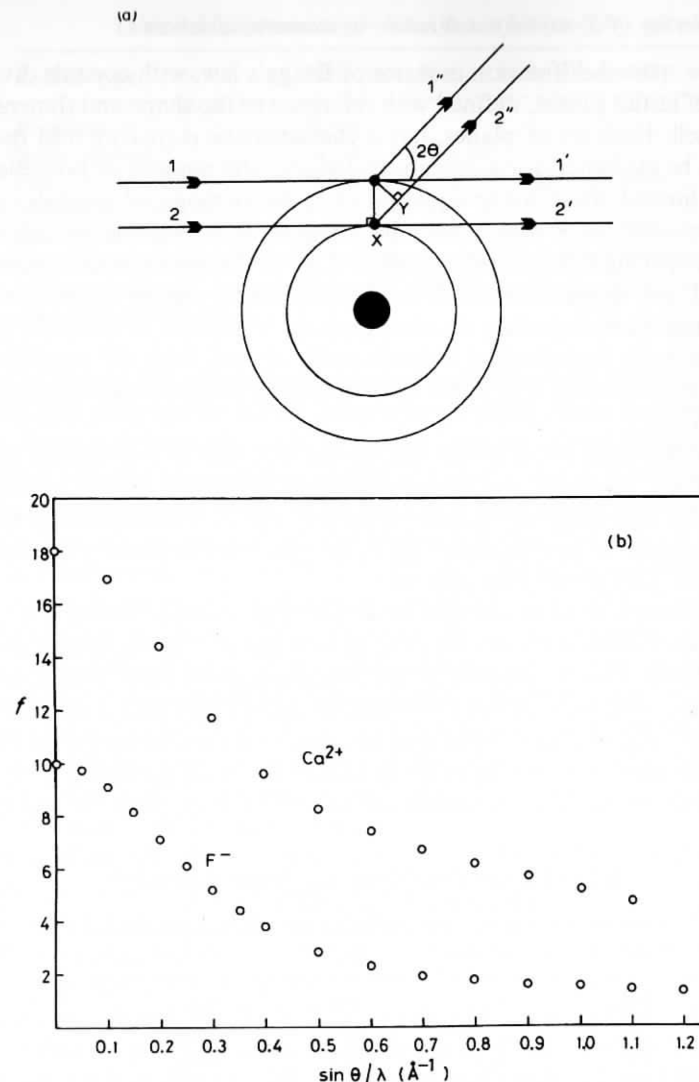

Fig. 3.14 (a) Scattering of X-rays by electrons in an atom. (b) Form factors of Ca^{2+} and F^-

readily because they determine the phase of diffracted beams, and this helps towards placing the remaining atoms. Because of their similar atomic numbers, Al and Si are difficult to distinguish, which may cause problems in determinations of aluminosilicate structures. One advantage of using neutrons instead of (or as well as) X-rays for crystallographic work is that the neutron form factors are not a simple function of atomic number. Light atoms, e.g. especially H and Li, are often strong neutron scatterers.

ii) *Scattering of X-rays by a crystal—systematic absences*

Earlier, we treated diffraction in terms of Bragg's law, with crystals divided up into sets of lattice planes, defined with reference to the shape and dimensions of the unit cell. Each set of planes, has a characteristic d-spacing and the Bragg angle can be evaluated for a given wavelength. The number of possible sets of planes is limited since, using equation (1.1) for orthogonal crystals, i.e. with $\alpha = \beta = \gamma = 90°$, h, k and l must be integers. It is possible to calculate all possible d-spacing values from equation (1.1) or the appropriate equations for other unit cell shapes, although the calculation is usually terminated when either a minimum d-spacing or maximum set of indices is reached. This has been done for a hypothetical orthorhombic crystal, with all possible h, k, l combinations of 0 and 1, in Table 3.4. Obviously, the list could be extended for higher indices.

In principle, each set of lattice planes can give rise to a diffracted beam. In practice, the intensity of the beams diffracted by certain sets of lattice planes may be zero. These are known as *systematic absences*. Systematic absences arise if the lattice type is non-primitive (I, F, etc.) or if elements of space symmetry (screw axes, glide planes) are present.

As an example of absences due to lattice type, consider α-Fe, Fig. 3.15(a), which is *bcc*. Reflection from the (100) planes has zero intensity and is systematically absent. This is because, at the Bragg angle for these planes, the body centre atoms which lie midway between adjacent (100) planes diffract X-rays exactly 180° out of phase relative to the corner atoms which lie on the (100) planes. Averaged over the whole crystal, there are equal numbers of corner and body centre atoms and the beams diffracted by each cancel completely. In

Table 3.4 *Calculated d-spacings for an orthorhombic cell, for a = 3.0, b = 4.0, c = 5.0 Å*

hkl	d (Å)	*hkl*	d (Å)
001	5.00	101	2.57
010	4.00	110	2.40
011	3.12	111	2.16
100	3.00		

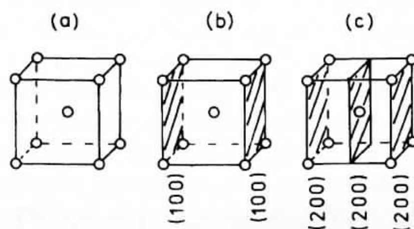

Fig. 3.15 (a) *bcc* α-Fe, (b) (100) planes, (c) (200) planes

Table 3.5 *Systematic absences due to lattice type*

Lattice type	Rule for reflection to be observed*
Primitive, P	None
Body centred, I	hkl; $h+k+l=2n$
Face centred, F	hkl; h, k, l **either all** odd or all even
Side centred, e.g. C	hkl; $h+k=2n$
Rhombohedral, R	hkl; $-h+k+l=3n$ or $(h-k+l=3n)$

* If space symmetry elements are present, **additional** rules may apply. These are not dealt with here.

contrast, a strong 200 reflection is observed because all the atoms lie on (200) planes (c) and there are no atoms lying between (200) planes to cause destructive interference. It is easy to show, by similar arguments, that the 110 reflection is observed whereas 111 is systematically absent in α-Fe. For each non-primitive lattice type there is a simple characteristic formula for systematic absences, Table 3.5. For a body centred cell, reflections, for which $(h+k+l)$ is odd, are absent, e.g. reflections such as 100, 111, 320, etc., are systematically absent.

Systematic absences are an extreme case of destructive interference between X-ray beams diffracted by individual atoms. They arise when one set of atoms diffracts X-rays that are exactly out of phase with those diffracted by a second set of atoms of the same type. Two conditions must be met for systematic absences: the diffracted beams must be out of phase (by $\lambda/2$ or π) and of the same amplitude (determined by scattering powers, f). In cases where destructive interference is not complete and intensities are actually observed, then one or both of these conditions is not met.

Let us consider now the rock salt structure. It is *fcc* and therefore, only those reflections for which h, k, l are either all odd or all even may be observed (Table 3.5). From this rule, for instance, (110) is systematically absent. In Fig. 3.16(a), (110) planes have Na^+ and Cl^- ions on the planes but equal numbers of the same ions are midway between the planes. Both conditions specified above are met and complete cancellation occurs. For the (111) planes, however, Na^+ ions lie on the planes and Cl^- ions lie exactly midway between them. Hence, the Na^+ and Cl^- ions scatter exactly 180° out of phase with each other for these planes, but since they have different scattering powers the destructive interference that occurs is only partial. The intensity of the (111) reflection in materials that have the rock salt structure is, therefore, related to the difference in atomic number of anion and cation. For the potassium halides, the (111) intensity is zero for KCl, since K^+ and Cl^- are isoelectronic, and its intensity should increase in the order:

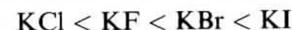

$$KCl < KF < KBr < KI$$

Some data which confirm this are given in Table 3.3.

Similar effects occur in other simple structures. In primitive cubic CsCl, if the difference between caesium and chlorine is ignored the atomic positions are the

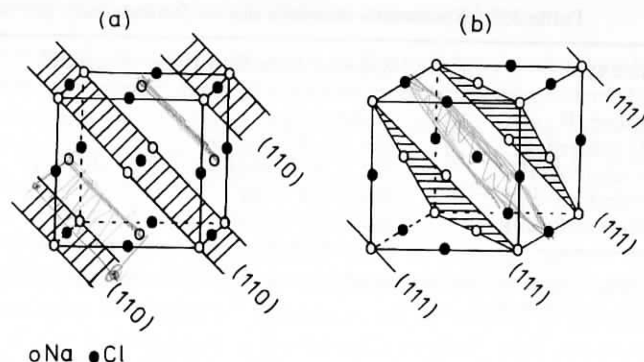

Fig. 3.16 (a) (110) and (b) (111) planes in NaCl

same as in body centred α-Fe, Fig. 3.15. The (100) reflection is systematically absent in α-Fe but is observed with CsCl because the scattering powers of Cs^+ and Cl^- are different, i.e. $f_{Cs^+} \neq f_{Cl^-}$.

iii) General formula for phase difference, δ

Each atom in a crystal scatters X-rays by an amount related to the scattering power, *f*, of that atom. In summing the individual waves to give the resultant diffracted beam, both the *amplitude* and *phase* of each wave are important. If we know the atomic positions in the structure, the amplitude and phase appropriate to each atom in the unit cell may be calculated and the summation carried out by various mathematical methods, therefore simulating what happens during diffraction. Let us consider first the relative phases of different atoms in the unit cell. In Fig. 3.17(a) are drawn two (100) planes of a crystal that has an orthogonal unit cell. Atoms A, B, C, A′ lie on the *a* axis (perpendicular to (100) planes) with A and A′ at the origin of adjacent unit cells. For the 100 reflection, A and A′ scatter in phase because their phase difference is exactly one wavelength, 2π radians (Bragg's law). Atom B, situated halfway between adjacent (100) planes, has fractional *x* coordinate (relative to A) of $\frac{1}{2}$. The phase difference between (waves diffracted from) A and B is $\frac{1}{2}\cdot 2\pi = \pi$, i.e. atoms A and B are exactly out of phase. Atom C has a general fractional coordinate *x* (at distance *xa* from A) and, therefore, a phase relative to A of $2\pi x$ (b).

Consider, now, the (200) reflection for the same unit cell (c). Since $d_{200} = \frac{1}{2}d_{100}$, then from Bragg's Law, $\sin\theta_{200} = 2\sin\theta_{100}$ and therefore $\theta_{200} \gg \theta_{100}$. Atoms A and B have a phase difference of 2π for the (200) reflection and scatter in phase, whereas their phase difference is π for the (100) reflection. Thus, the effect of halving *d* is to double the relative phase difference between pairs of atoms such as A and B; therefore, A and C have a phase difference of $(2x \cdot 2\pi)$ for the (200) reflection.

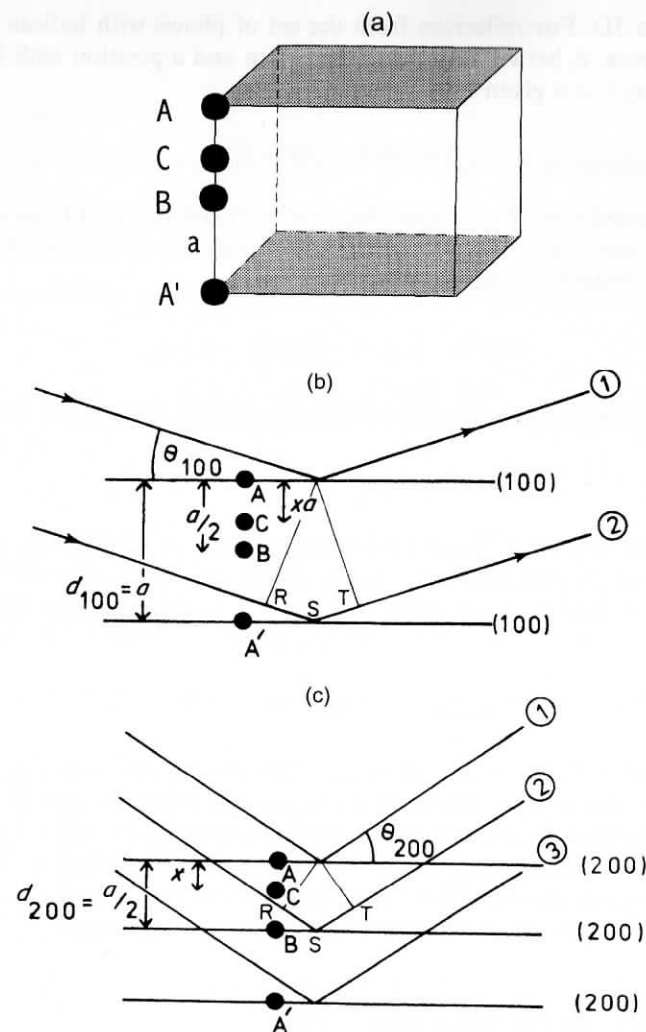

Fig. 3.17 (a, b) (100) planes for an orthogonal unit cell ($\alpha = \beta = \gamma = 90°$). Atoms A, B, C, A′ lie on the *a* cell edge. (c) (200) planes for the same unit cell as in (a, b)

For the general case of an *h*00 reflection, the *d*-spacing between adjacent (*h*00) planes is $(1/h)a$ and the *phase difference*, δ, between A and C is given by

$$\delta = 2\pi hx \qquad (3.6)$$

The phase difference between atoms depends, therefore, on two factors: the indices of the reflection that is being considered and the fractional coordinates of the atoms in the unit cell. This reasoning may be extended readily to

diffraction in 3D. For reflection from the set of planes with indices (*hkl*), the phase difference, δ, between atoms at the origin and a position with fractional coordinates x, y, z is given by

$$\delta = 2\pi(hx + ky + lz) \tag{3.7}$$

This important formula is applicable to all unit cell shapes. Let us use it on a simple structure, γ-Fe, which is *fcc* with atoms at the corner and face centre positions, i.e. with fractional coordinates:

$$0,0,0;\quad \tfrac{1}{2},\tfrac{1}{2},0;\quad \tfrac{1}{2},0,\tfrac{1}{2};\quad 0,\tfrac{1}{2},\tfrac{1}{2}$$

These coordinates may be substituted into the formula for δ to give four phases:

$$0,\ \pi(h+k),\ \pi(h+l),\ \pi(k+l)$$

How do these vary? If h, k and l are either all even or all odd, the phases are in multiples of 2π and, therefore, are in phase with each other. If, however, one, say h, is odd and the other two, k and l, are even, the four phases reduce to

$$0, (2n+1)\pi,\ (2n+1)\pi,\ 2n\pi$$

The first and last are π out of phase with the middle two and complete cancellation occurs. The γ-Fe structure is a simple example of an *fcc* lattice in which the Fe atoms correspond to lattice points; we have in fact just proved the condition for systematic absences due to face centring! (Table 3.5). The reader may like to prove the condition for systematic absences in a *bcc* structure by working out the phases of the atoms for the structure of α-Fe.

iv) Intensities and structure factors

Let us now generalize the treatment to consider any atom, j in the unit cell. The diffracted wave of amplitude f_j and phase δ_j is a sine wave of the form

$$F_j = f_j \sin(\omega t - \delta_j) \tag{3.8}$$

The waves diffracted from each atom in the cell have the same angular frequency, ω, but may differ in f and δ. The resultant intensity is obtained from the summation of the individual sine waves. Mathematically, addition of waves may be carried out by various methods, including vector addition and the use of complex numbers. In complex notation, wave j may be written as

$$F_j = f_j(\cos\delta_j + i\sin\delta_j) \tag{3.9}$$

or as

$$F_j = f_j \exp(i\delta_j) \tag{3.10}$$

where $i = \sqrt{-1}$
The intensity of a wave is proportional to the square of its amplitude; i.e.

$$I \propto f_j^2 \tag{3.11}$$

and is obtained by multiplying the equation for the wave by its complex conjugate; i.e.

$$I \propto f_j \exp(i\delta_j) \cdot f_j \exp(-i\delta_j)$$

and therefore

$$I \propto f_j^2$$

Alternatively,

$$[f_j(\cos\delta_j + i\sin\delta_j)][f_j(\cos\delta_j - i\sin\delta_j)] = f_j^2(\cos^2\delta_j + \sin^2\delta_j) = f_j^2$$

Substituting the expression for δ, the equation of a diffracted wave becomes

$$\begin{aligned} F_j &= f_j \exp 2\pi i(hx_j + ky_j + lz_j) \\ &= f_j[\cos 2\pi(hx_j + ky_j + lz_j) + i\sin 2\pi(hx_j + ky_j + lz_j)] \end{aligned} \tag{3.12}$$

When written in this form, the summation over the j atoms in the unit cell may be carried out readily, to give the *structure factor* or *structure amplitude*, F_{hkl}, for the *hkl* reflection; i.e.

$$F_{hkl} = \sum_{j=1\to n} [f_j \exp(i\delta_j)]$$

or

$$F_{hkl} = \sum_j f_j(\cos\delta_j + i\sin\delta_j) \tag{3.13}$$

The intensity of the diffracted beam I_{hkl} is proportional to $|F_{hkl}|^2$ and is obtained from

$$\begin{aligned} I_{hkl} \propto |F_{hkl}|^2 &= \left[\sum_j f_j(\cos\delta_j + i\sin\delta_j)\right]\left[\sum_j f_j(\cos\delta_j - i\sin\delta_j)\right] \\ &= \sum_j (f_j\cos\delta_j)^2 + \sum_j (f_j\sin\delta_j)^2 \end{aligned} \tag{3.14}$$

This latter is a very important formula in crystallography because, using it, the intensity of any *hkl* reflection may be calculated from a knowledge of the atomic coordinates in the unit cell. Let us see one example of its use. Calcium fluoride, CaF_2, has the fluorite structure with atomic coordinates in the *fcc* unit cell:

$$\begin{array}{lllll} \text{Ca} & 0,0,0 & \frac{1}{2},\frac{1}{2},0 & \frac{1}{2},0,\frac{1}{2} & 0,\frac{1}{2},\frac{1}{2} \\ \text{F} & \frac{1}{4},\frac{1}{4},\frac{1}{4} & \frac{1}{4},\frac{1}{4},\frac{3}{4} & \frac{1}{4},\frac{3}{4},\frac{1}{4} & \frac{3}{4},\frac{1}{4},\frac{1}{4} \\ & \frac{3}{4},\frac{3}{4},\frac{1}{4} & \frac{3}{4},\frac{1}{4},\frac{3}{4} & \frac{1}{4},\frac{3}{4},\frac{3}{4} & \frac{3}{4},\frac{3}{4},\frac{3}{4} \end{array}$$

Substitution of these coordinates into (3.13), yields

$$\begin{aligned} F_{khl} = & f_{\text{Ca}}[\cos 2\pi(0) + \cos\pi(h+k) + \cos\pi(h+l) + \cos\pi(k+l)] \\ & + if_{\text{Ca}}[\sin 2\pi(0) + \sin\pi(h+k) + \sin\pi(h+l) \\ & + \sin\pi(k+l)] + f_{\text{F}}[\cos\pi/2(h+k+l) \\ & + \cos\pi/2(h+k+3l) + \cos\pi/2(h+3k+l) \\ & + \cos\pi/2(3h+k+l) + \cos\pi/2(3h+3k+l) \\ & + \cos\pi/2(3h+k+3l) + \cos\pi/2(h+3k+3l) \\ & + \cos\pi/2(3h+3k+3l)] + if_{\text{F}}[\sin\pi/2(h+k+l) \\ & + \sin\pi/2(h+k+3l) + \sin\pi/2(h+3k+l) + \sin\pi/2(3h+k+l) \\ & + \sin\pi/2(3h+3k+l) + \sin\pi/2(3h+k+3l) \\ & + \sin\pi/2(h+3k+3l) + \sin\pi/2(3h+3k+3l)] \end{aligned}$$

Since the fluorite structure is *fcc*, h, k and l must be all odd or all even for an observed reflection; for any other combination, $F = 0$ (try it!). Consider the reflection 202:

$$\begin{aligned} F_{202} = & f_{\text{Ca}}(\cos 0 + \cos 2\pi + \cos 4\pi + \cos 2\pi) \\ & + if_{\text{Ca}}(\sin 0 + \sin 2\pi + \sin 4\pi + \sin 2\pi) \\ & + f_{\text{F}}(\cos 2\pi + \cos 4\pi + \cos 2\pi + \cos 4\pi + \cos 4\pi + \cos 6\pi \\ & + \cos 4\pi + \cos 6\pi) + if_{\text{F}}(\sin 2\pi + \sin 4\pi + \sin 2\pi + \sin 4\pi + \sin 4\pi \\ & + \sin 6\pi + \sin 4\pi + \sin 6\pi) \end{aligned}$$

That is,

$$\begin{aligned} F_{202} = & f_{\text{Ca}}(1+1+1+1) + if_{\text{Ca}}(0+0+0+0) \\ & + f_{\text{F}}(1+1+1+1+1+1+1+1) \\ & + if_{\text{F}}(0+0+0+0+0+0+0+0) \end{aligned}$$

i.e.

$$F_{202} = 4f_{\text{Ca}} + 8f_{\text{F}}$$

The 202 reflection in CaF_2 has a d-spacing of 1.929 Å ($a = 5.464$ Å). Therefore

$$\theta_{202} = 23.6^\circ \text{ and } \sin\theta/\lambda = 0.259 \text{ for } \lambda = 1.5418 \text{ Å (Cu } K\alpha)$$

Form factors for Ca and F are given in Fig. 3.14(b); for $\sin\theta/\lambda = 0.259$, by interpolation,

$$f_{\text{Ca}} = 12.65 \quad \text{and} \quad f_{\text{F}} = 5.8$$

Therefore,

$$F_{202} = 97$$

This calculation may be made for a series of *hkl* reflections and the results, after scaling, compared with the observed values, Table 3.6. In solving unknown structures, the objective is always to obtain a model structure for which the calculated structure factors, F_{hkl}^{calc}, are in good agreement with experimental values i.e. F_{hkl}^{obs}.

An important feature which simplifies the above calculations is that all the sine terms are zero. This is because the origin of the unit cell is also a centre of symmetry. For each atom at position x, y, z there is a centrosymmetrically related atom at $-x, -y, -z$ (e.g. F at $\frac{1}{4},\frac{1}{4},\frac{1}{4}$ and $-\frac{1}{4}-\frac{1}{4}-\frac{1}{4}$, i.e. $1-\frac{1}{4}, 1-\frac{1}{4}, 1-\frac{1}{4}$ or $\frac{3}{4},\frac{3}{4},\frac{3}{4}$) and since $\sin(-\delta) = -\sin\delta$, the summation of the sine terms over the unit cell contents is zero. If, on the other hand, one of the F atoms was taken as the origin of the cell, the sine terms would be non-zero because, F, with its immediate coordination environment of 4Ca arranged tetrahedrally, does not lie on a centre of symmetry. Many structures, of course, belong to non-centric space groups, in which case the complete calculation of F using both cosine and sine terms cannot be avoided.

v) *R-factors and structure determination*

It was shown above how the structure factor, F_{hkl}^{calc}, may be calculated for any *hkl* reflection from a knowledge of the coordinates of the atoms in the unit cell. The values of F_{hkl}^{calc} for the first five lines in the powder pattern of CaF_2 are given in Table 3.6. The experimental intensities, the intensities after correction for the L_p factor and *multiplicities* and the observed structure factor, F_{hkl}^{obs}, given by: $F_{hkl}^{\text{obs}} = \sqrt{I_{\text{corr}}}$, are also listed. In order to compare the values of F_{hkl}^{obs} and F_{hkl}^{calc}, they are scaled such that $\sum F_{hkl}^{\text{obs}} = \sum F_{hkl}^{\text{calc}}$. Multiplication of each F_{hkl}^{obs} value by 141 gives the scaled values listed. The measure of agreement between the individual, scaled F_{hkl}^{obs} and F_{hkl}^{calc} values is given by the *residual factor* or *R-factor*, defined by:

$$R = \frac{\sum \| F^{\text{obs}} | - | F^{\text{calc}} \|}{\sum |F^{\text{obs}}|} \tag{3.15}$$

An R-factor of 0.15 (or 15 per cent after multiplying by 100) is obtained.

Table 3.6 Structure factor calculations for CaF_2: X-ray powder diffraction

d (Å)	hkl	I	Multiplicity*	$I/(\text{multiplicity} \times L_p)$†	F^{obs}	F^{calc}	F^{obs} scaled	$\lVert F^{obs}\rvert - \lvert F^{calc}\rVert$
3.143	111	100	8	0.409	0.640	67	90	23
1.929	202	57	12	0.476	0.690	97	97	0
1.647	311	16	24	0.098	0.313	47	44	3
1.366	400	5	6	0.193	0.439	75	62	13
1.254	331	4	24	0.047	0.217	39	31	8

$\sum F^{obs}\text{scaled} = 324$

$\sum \lVert F^{obs}\rvert - \lvert F^{calc}\rVert = 47$

$R = \frac{\sum \lvert \Delta F \rvert}{\sum F^{obs}} = \frac{47}{324} = 0.15$

* The multiplicity of an X-ray powder line is the number of equivalent sets of planes that diffract at the same Bragg angle. Thus, overlapping with 111 are $\bar{1}11$, $1\bar{1}1$, $11\bar{1}$, $\bar{1}\bar{1}1$, $\bar{1}1\bar{1}$, $1\bar{1}\bar{1}$ and $\bar{1}\bar{1}\bar{1}$, where a negative index indicates that a negative crystallographic direction was used in defining it.

† The Lorentz polarization factor, L_p, is an angular correction factor that includes the effect of equation (3.5) and certain instrumental factors. Available from standard tables.

In solving unknown structures, one is guided, among other things, by the value of R; the lower it is, the more likely is the structure to be correct. The calculation given for CaF_2 is rather artificial since only five reflections were used (normally, hundreds or thousands are used), but it serves as an illustration. It is not possible to give hard and fast rules linking the magnitude of R and the likely correctness of a structure, but, usually, when R is less than 0.1 to 0.2, the proposed structure is essentially correct. A structure which has been solved fully using good quality intensity data has R typically in the range 0.02 to 0.06.

l) Electron density maps

An electron density map shows the variation of electron density throughout the unit cell. When solving an unknown structure it is often useful to construct electron density maps (Fourier maps) in order to try and locate atoms. As the structure refinement proceeds, the quality of the electron density map usually improves: the background electron density decreases and more peaks due to individual atoms become resolved. We are concerned here, not with the methods of structure refinement but only with the results, and the electron density map obtained at the end of a structure determination is an important piece of information. Electron density maps take the form of sections through the structure at regular intervals; by superposing these, a 3D picture of the electron density distribution may be obtained. In Fig. 3.18 is shown the electron

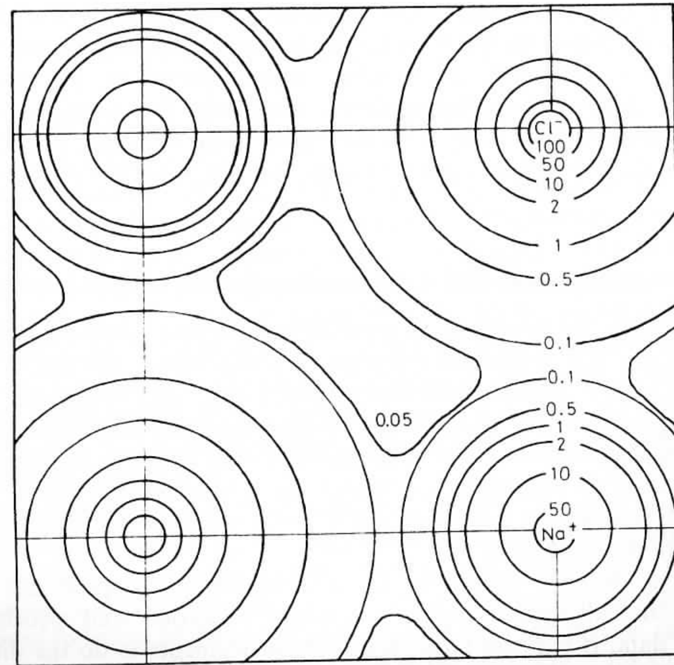

Fig. 3.18 Electron density map for NaCl

density distribution for a section through a very simple structure, NaCl. The section is parallel to one unit cell face and passes through the centres of the Na^+, Cl^- ions. It has the following features.

An electron density map resembles a geographical contour map. The contours are lines of constant electron density throughout the structure. Electron density maxima correspond to atoms; the coordinates of the atoms in the unit cell are given by the coordinates of the peak maxima. The peak height is proportional to the number of electrons possessed by that atom, which apart from very light atoms equals the atomic number of that atom. In Fig. 3.18, peaks of relative height 100 and 50 are seen and are assigned to Cl and Na, respectively. (The atomic numbers of Cl and Na are 17 and 11; for ions, the number of electrons are 18 and 10. The experimental maxima are therefore in fair agreement with the expected values.)

Electron density maps also show that our mental picture of atoms as spheres is essentially correct, at least on a time average. The electron density drops to almost zero at some point along the line connecting pairs of adjacent atoms in Fig. 3.18 and this supports the model of ionic bonding in NaCl. In structures which have covalent bonding, there is residual electron density between atoms on the electron density map. However, in other than very simple structures, such as the alkali halides, it is difficult to use electron density maps to determine quantitatively the distribution of valence electrons. In most structure refinements, both the position and thermal vibration factors of atoms are varied in order to achieve the best agreement between measured and calculated structure factors. The final parameters may represent a compromise, therefore, and the electron density map, which is greatly influenced by the thermal vibration factors, is not necessarily an absolute representation of the distribution of valence electrons. In refining simple structures, the atomic coordinates are usually known accurately. This then gives more accuracy to the thermal vibration factors (or *temperature factors*) and hence to the electron density map.

m) X-ray crystallography and structure determination—what's involved?

For determining the structures of crystalline materials, X-ray crystallography reigns supreme. For molecular materials, it complements the use of spectroscopic techniques—NMR, mass spectroscopy, etc.—and often, one may use either crystallography or spectroscopy to determine molecular structures. For non-molecular materials, or for molecular materials whose arrangement in the crystalline state is important, or whose bond lengths and angles must be determined, then X-ray crystallography is by far the most important technique for structure determination.

Nowadays, solving structures is mathematically complex but usually highly automated with computer-controlled collection and processing of diffraction data. It requires large, expensive instruments to do the diffraction experiments and is time-consuming: given a reasonable-sized single crystal, several days are often required to collect the data and at least a few hours

of computation to solve the structure. It is not yet the kind of experiment that is carried out in an afternoon in a laboratory, but nevertheless, it is important to have at least a passing familiarity with the processes and problems involved. In fact, we have already covered much of the groundwork earlier in this chapter.

Solving an unknown structure is a bit like solving a set of simultaneous equations. The unknowns are the atomic coordinates and the equations are the experimental intensity data. Obviously, we must have at least as many equations (i.e. intensities) as variables but in practice, we need many more intensities than variables to obtain good quality structure determinations. This is partly because the intensity data may have errors, partly because the computational methods involve statistical analyses of data which function properly only with large data sets, and partly because the Fourier methods used in structure determination are effective only with a large number of coefficients (intensities). Let us see some examples with structures of varying complexity, because the number of variables to be determined dictates the type of diffraction experiment that is required.

First, suppose that we have material, MX_2, suspected to have the rutile structure: how many variables must be determined in order to confirm the structure? From the rutile structure, Fig. 1.32, atoms M are in fixed positions, at the corner and body centre and hence have no positional variables. The atoms, X, have a single positional variable, x, since the coordinates of the four atoms in the unit cell are given by:

$$x, x, 0; \quad 1-x,\ 1-x, 0; \quad \tfrac{1}{2}-x, \tfrac{1}{2}+x, \tfrac{1}{2}; \quad \tfrac{1}{2}+x, \tfrac{1}{2}-x, \tfrac{1}{2}$$

Hence, once x has been determined, all four atoms have been located. (Note, for TiO_2, Fig. 1.32, $x = 0.3$.)

In addition to the positional variables, atoms vibrate, either isotropically or anisotropically and the *temperature factors* are additional variables which must be determined in any good quality structure refinement. The first stage is to determine *isotropic temperature factors*, B_{iso}, which assumes that the atoms are vibrating isotropically; there are two of these for rutile, one for M and one for X. In many cases, determination of positional coordinates and B_{iso} values is sufficient. In order to determine these accurately, intensities of at least 10–20 reflections would normally be required; since the powder X-ray pattern may contain at least this number of lines, the structure could be determined satisfactorily from powder data.

Second, a moderately complex structure is that of $YBa_2Cu_3O_x$, the so-called YBCO or Y123 ceramic superconductor. It is orthorhombic with a structure related to but rather more complex than that of perovskite. The unit cell contains one formula unit with $x = 7.0$. There are 5 positional variables to be determined to locate all the atoms and $8B_{iso}$ values (4 for oxygen, since there are four crystallographically distinct oxygens in the structure, 2 for Cu and 1 each for Ba, Y). One of the oxygens is present in variable amounts (x is variable in

the formula) and the fractional occupancy of its site is a variable. This gives a total of 14 variables and for a good structure determination, 200–300 intensities would be required. Routine powder methods do not give this number of well-resolved reflections; either special powder techniques, such as high-resolution neutron or X-ray diffraction, or single crystal methods must be used. In these, the data set is increased both by collecting data to lower *d*-spacings using shorter-wavelength radiation and, with single crystals, by recording data that are too weak to appear in powder patterns.

Third, for yet more complex structures, such as many silicates and complex organic molecules, especially if they are of low symmetry, the number of variables may be 50–100 and single crystal data, giving perhaps 2,000 to 3,000 intensities, are usually essential.

Once the intensity data have been collected, corrected for factors such as Lorentz polarization and converted to observed structure factors, the process of solving the structure can begin. The problem is essentially to determine the values of the atomic coordinates x, y, z that, when substituted into equation (3.12), yield calculated F values that match the observed ones.

In cases where both the signs (+or−) and magnitudes of the F^{obs} values are known, there are standard mathematical procedures, based on Fourier series, for attacking this problem. This is because the observed diffracted X-ray beams may be combined mathematically, as a Fourier transform, to give the crystal structure in the form of an electron density map (as in Fig. 3.18). The relevant equation is:

$$\rho(u, v, w) = \frac{1}{V}\sum_h\sum_k\sum_l F_{hkl}\cos 2\pi(hu + kv + lw) \qquad (3.16)$$

from which, for any point u, v, w in the unit cell, the electron density, ρ, is calculated by substituting into the summation all the observed F and h, k, l values. In order to obtain a good quality map, there must be a large number of terms in the summation and this is the main reason why the number of intensity values required for a structure determination is much greater than the number of variables.

There is a clear analogy between this mathematical addition and the production of images in optical and electron microscopes. In microscopes, the diffraction pattern obtained by shining a beam of either light or electrons on the sample, is combined to give an image using either an optical lens or an electromagnetic lens. There is, unfortunately, no material that can act as an 'X-ray lens' and we must resort to mathematical methods to perform this combination. This brings us to the key problem in crystallography: while the amplitudes of the F^{obs} values are determined directly and unequivocally from the intensities, their phases are not. Thus, while the I values must be positive, the F values, given by $\sqrt{I}$, may be positive or negative. Many means have been devised to attack this '*phase problem*'. The most successful ones are outlined next.

i) The Patterson method

This method uses a Fourier summation rather similar to equation (3.16) but in which intensity (or F^2_{hkl}) data form the *coefficients*, i.e.

$$P(u, v, w) = \frac{1}{V}\sum_h\sum_k\sum_l |F_{hkl}|^2\cos 2\pi(hu + kv + lw) \qquad (3.17)$$

The resulting Patterson map looks similar to a Fourier map, but the regions of high electron density correspond to vectors between pairs of atoms. The peak heights are proportional to the products of the atomic numbers; hence, vectors formed from pairs of the heaviest atoms in the unit cell give rise to the largest peaks. The peak positions give the separation, vectorially, of these two atoms in the structure. Thus, two atoms at x_1, y_1, z_1 and x_2, y_2, z_2 will give a Patterson peak, relative to the origin of the Patterson map, at $x_1 - x_2, y_1 - y_2, z_1 - z_2$. This does not give the positions of heavier atoms directly, but it does give their relative positions in the unit cell and this is often of great assistance in getting started: thus, if one atom can be located with confidence, then the Patterson map may suggest the location of others. Once such a start has been made, other Fourier methods may be used to complete the structure determination.

ii) Fourier methods

These may be used even though the complete list of F^{obs} values, with their signs, is not available. Use is made of composite F values, whose magnitudes are taken from the F^{obs} listing and whose signs are taken from a partial structure factor calculation based on the heavy atom positions only. Since the heavy atoms scatter X-rays most strongly, they are likely to dominate the intensities and, in particular, control the phases (i.e. whether + or −). Hence, most of the signs can probably be determined correctly at this stage, especially for the larger F values. A Fourier map, made from equation (3.16) and these composite F values, should then reveal considerably more electron density peaks and enable lighter atoms to be located. This process may be repeated: a more accurate structure factor calculation is performed using the more extensive list of atomic coordinates obtained from the Fourier map; consequently, the signs of more F values are determined correctly and an improved Fourier map can be calculated.

Once most of the atoms have been located approximately, *least squares refinement* procedures may be used to improve the agreement between F^{obs} and F^{calc} and thereby, minimize the R-factor, equation (3.15). In these procedures, atom positions are permitted to vary somewhat, the effect on R is noted and the optimum positions (for minimum R) are found by trial and error. It is also useful to construct a *difference Fourier map* using ($F^{obs} - F^{calc}$) values as the coefficients:

$$\Delta(u, v, w) = \frac{1}{V}\sum_h\sum_k\sum_l (F^{obs} - F^{calc}) \cos 2\pi(hu + kv + lw) \qquad (3.18)$$

A difference map may show regions of low, positive electron density associated with previously undetected light atoms such as H. Or, it may show regions of negative electron density, indicating that an atom has been wrongly placed at that position. Or it may be completely featureless, indicating that the structure refinement is correct and complete.

iii) Direct methods

These are very useful for structure determination and work best when all the component atoms have similar atomic number, thus complementing the Patterson method which works best when a small number of heavy atoms are present. Direct methods are used to determine phases. They are based on the statistical probabilities of phases being either + or −. For example, for centrosymmetric structures, the *Sayre probability relationship* indicates that for three reflections h, k, l, h', k', l' and h'', k'', l'' that are related by $h'' = h - h'$, $k'' = k - k'$ and $l'' = l - l'$, then the sign of one phase is likely to be the same as the product of the signs of the other two. Thus, if 312 and 111 are both−, then 201 is probably +. By choosing three reflections, whose phases are not known, there are eight possible combinations of + and −. For each combination, the phases of other reflections may be predicted. A range of methods are available for predicting phases and optimizing the value of the predictions. The end result is an *E-map*, similar to an electron density map and from which atomic positions may be determined.

3.4 Electron diffraction

Electrons have wave characteristics which allow them to be used for diffraction experiments. Their wavelength is related to velocity, which is governed by the voltage through which they are accelerated in an 'electron gun' and is usually about 0.04 Å in conventional electron microscopes. The two techniques of *electron diffraction* and *electron microscopy* are closely related. The latter is used more widely and is discussed in Chapter 4; here we shall see briefly the general characteristics of electron diffraction and how it compares with X-ray diffraction.

Electrons interact strongly with matter and intense diffraction patterns are obtained from very small samples; indeed, for transmission studies, the samples should not be thicker than about 100 nm (1 nm = 10 Å), otherwise the electrons may not pass through the sample. This contrasts markedly with X-ray diffraction: the efficiency with which X-rays are diffracted by matter is low and, for single crystal studies, relatively large crystals, 0.05 mm or greater in dimensions are required.

One disadvantage of electron diffraction is that *secondary diffraction* commonly occurs. Because the scattering efficiency of electrons is high, the

diffracted beams are strong. Secondary diffraction occurs when these diffracted beams effectively become the incident beam and are diffracted by another set of lattice planes. There are two undesirable consequences of secondary diffraction. First, under certain circumstances, extra reflections may appear in the diffraction pattern; care is therefore needed in their interpretation. Second, the intensities of diffracted beams are unreliable and cannot be used quantitatively for structure determination.

In spite of these disadvantages, electron diffraction is very useful and complements the various X-ray techniques. Thus with X-rays, the scattering efficiency is small, secondary diffraction is rarely a problem and intensities are reliable, but (relatively) large samples are needed. With electrons, the scattering efficiency is high and intensities are unreliable, but very small samples can be studied. The technique is very useful for obtaining unit cell and space group information for crystals smaller than 0.01 to 0.02 mm in diameter; it is, in fact, the only reliable method for obtaining such information. Other methods such as graphical or computer-assisted indexing of X-ray powder patterns, give results that are not always 100 per cent reliable. In spite of its utility, electron diffraction is underused in solid state chemistry for unit cell and space group determination.

Electron diffraction is unsuitable as a routine method of phase identification in relatively large (e.g. 10 mg or more) samples. It is useful, however, (a) when very small quantities are available, (b) for thin film samples, and (c) for detecting small amounts of impurity phases. In all these cases, there would be insufficient material to show up in X-ray diffraction.

3.5 Neutron diffraction

Neutron diffraction is a very expensive technique. In order to get a sufficiently intense source of neutrons, a nuclear reactor is needed. Few laboratories have their own neutron facility and, instead, experiments are carried out at central laboratories which provide a user service (e.g. at the ILL, Grenoble, France or the Argonne, USA). In spite of its high cost, neutron diffraction is a valuable technique and can provide information, especially on magnetic materials, that is not attainable with other techniques. Clearly, it is never used when alternative techniques, such as X-ray diffraction, can solve a particular problem.

Neutron beams are usually of low intensity and therefore the sample size required is relatively large, at least 1 mm^3. Since crystals of this size are often not available, crystallographic studies are usually carried out on polycrystalline samples. A powder neutron diffraction pattern looks very much like an X-ray one.

There are several characteristic differences between neutron and X-ray diffraction. First, the neutrons obtained from a nuclear reactor give a continuous spectrum of radiation, without the intense characteristic peaks that are present in X-ray spectra (as in Fig. 3.1b). The neutrons that are used for diffraction have wavelength of the order 0.5 to 3 Å. In order to have monochromatic neutrons for conventional diffraction experiments, it is necessary to select

a particular wavelength and filter out the remainder using a crystal monochromator. Most of the available neutron energy is wasted, therefore, and the beam that is used is weak and not particularly monochromatic.

A recent exciting advance uses pulsed neutron sources coupled with *time of flight* analysis. The neutrons are obtained using particle accelerators to bombard a heavy metal target with high-energy particles such as protons. The efficiency of the *spallation* process, yielding about 30 neutrons per proton, gives a high neutron flux suitable for diffraction experiments. In the time of flight method, the entire neutron spectrum (variable wavelength) is used with a fixed diffraction angle, θ. Neutron wavelength depends on velocity, given by the de Broglie relation, $\lambda = h/mv$, where m is the mass of the neutron, 1.675×10^{-27} kg. Hence, the diffracted radiation arriving at the detector is separated according to its time of flight and wavelength. The fundamental law of diffraction is again Bragg's law, $n\lambda = 2d\sin\theta$. In the time of flight method, λ and d (the d-spacing) are the variables at fixed θ. This compares with conventional diffraction techniques in which d and θ are the variables at fixed λ. The pulsed method gives rapid data collection. It may therefore also be used for studies of short time phenomena, especially in experiments where samples are subjected to pulsed magnetic fields.

A second difference between neutron and X-ray diffraction is that the scattering powers of atoms towards neutrons are quite different from those towards X-rays. In the latter, scattering power is a simple function of atomic number and light atoms such as hydrogen diffract X-rays only weakly. With neutrons, the atomic nuclei, rather than the extranuclear electrons, are responsible for the scattering and in fact, hydrogen is a strong scatterer of neutrons. There is no simple dependence of neutron scattering power on atomic number and additionally, some atoms cause a change of phase of π (or $\lambda/2$) in the diffracted neutron beam.

a) Crystal structure determination

Neutron diffraction may be used for crystallographic work in cases where X-ray diffraction is inadequate. It has been much used to locate light atoms, especially hydrogen in hydrides, hydrates and organic structures. Usually, the main part of the structure is solved by X-ray methods and neutron diffraction is used to locate the light atoms. Neutron diffraction is also used to distinguish atoms that have similar X-ray scattering powers, such as Mn, Fe, Co and Ni. The neutron scattering powers of these atoms are different and, for instance, superlattice phenomena, associated with Mn/Fe ordering in alloys, are readily observed by neutron diffraction.

b) Magnetic structure analysis

Magnetic properties depend on the presence of unpaired electrons, especially in d or f orbitals. Since neutrons possess a magnetic dipole moment, they interact with unpaired electrons and consequently, are diffracted by both atomic nuclei and unpaired electrons. This forms the basis of a powerful technique for studying the magnetic structure of materials. A simple example of magnetic structure and order is shown by NiO. By X-ray diffraction, NiO has the *fcc* rock salt structure. When examined by neutron diffraction, however, extra peaks are observed which indicate the presence of a superstructure. This arises because the unpaired d electrons (in the e_g orbitals) are arranged so as to be antiparallel in alternate layers of nickel atoms, Fig. 3.19. Neutrons detect this ordering of spins whereas X-rays do not. The unit cell of 'antiferromagnetic' NiO, which is stable below 250°C, has eight times the volume of paramagnetic NiO, stable above 250°C. The structure also shows a slight rhombohedral distortion, involving a contraction in the [111] direction perpendicular to the planes of ordered Ni^{2+} ions. This distortion is very small, however, and is detected by the splitting of reflections such as [111] and [$\bar{1}$11] only in high resolution neutron powder diffraction patterns. For present purposes, we may ignore this distortion and treat the structure, geometrically as cubic.

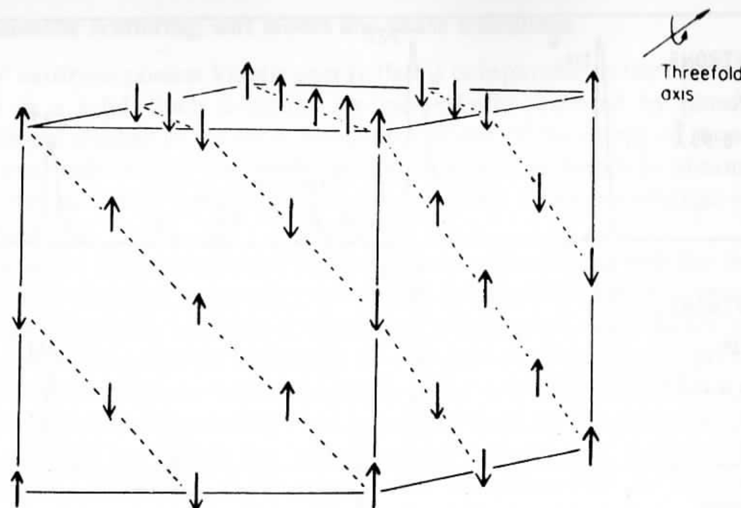

Fig. 3.19 Antiferromagnetic superstructure in MnO, FeO and NiO, showing pseudo-cubic unit cell for which a (supercell) = $2a$ (subcell). Oxygen positions are not shown

Neutron powder diffraction patterns for MnO (which behaves very similarly to NiO) below and above the Néel temperature, together with a schematic X-ray powder pattern at room temperature, are shown in Fig. 3.20. Comparison of the two patterns above T_N (b and c) shows that lines appear in the same positions but are of very different intensities. In the rock salt structure, the condition for reflection is that h, k, l should be either all odd or all even. Hence, the first four lines to be expected in the powder pattern are 111, 200, 220 and 311. All four lines appear in both patterns but 200 and 220 are weak in the neutron pattern (b). The small intensity of 200 and 220 in (b) is largely because the neutron scattering powers of Mn^{2+} and O^{2-} are opposite in sign although

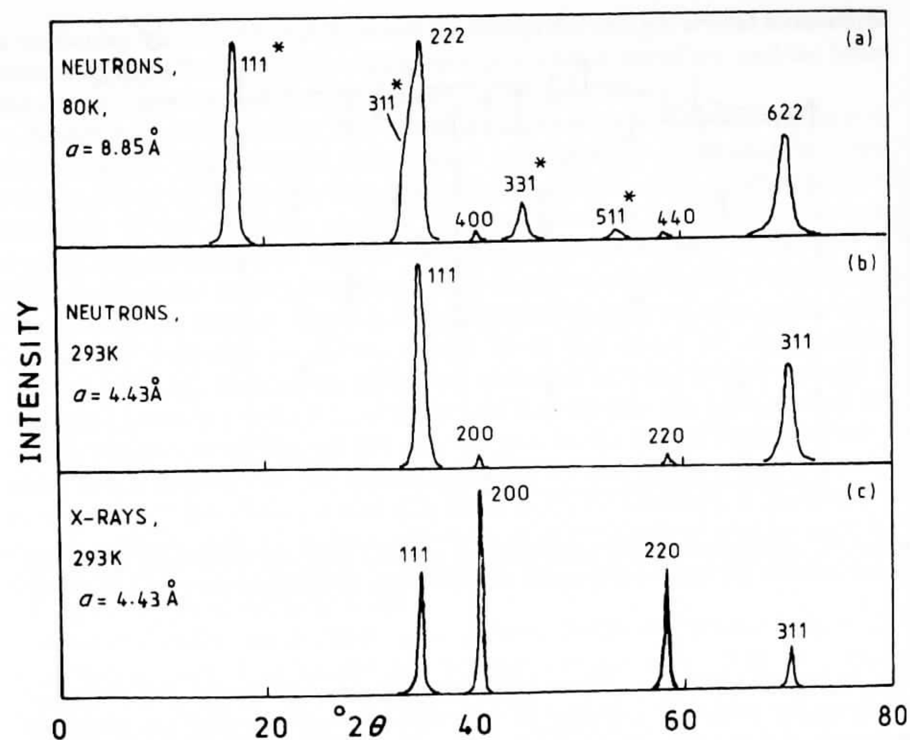

Fig. 3.20 Schematic neutron and X-ray powder diffraction patterns for MnO for $\lambda = 1.542$ Å. Peaks are assigned Miller indices for the cubic unit cells given. Neutron data are adapted from Shull, Strauser and Wollan, *Phys. Rev.*, **83**, 333, 1951. X-ray data are from Powder Diffraction File, Card No. 7-230

slightly different in magnitude. Partial cancellation therefore occurs for the 200 and 220 reflections since Mn^{2+} and O^{2-}. ions on the same planes scatter out of phase with each other. This is precisely the opposite of the case with scattering of X-rays, for which the scattering factors of all elements have the same sign and therefore for the 200 and 220 reflections, Mn^{2+} and O^{2-} scatter in phase with each other.

Comparison of (a) and (b) shows that below T_N extra lines (asterisked) appear in the neutron diffraction pattern. These extra lines are associated with the antiferromagnetic superstructure. Although, as mentioned above, the true symmetry of the antiferromagnetic structure is rhombohedral, to a first approximation it can be treated as cubic with cell dimensions that are twice the value for the high temperature paramagnetic structure, i.e. $a = 8.85$ Å at 80 K ($< T_N$) whereas at 293 K ($> T_N$), $a = 4.43$ Å. The volumes of the unit cells are therefore, in the ratio of 8:1. The extra lines in the powder pattern of the antiferromagnetic structure may be indexed as shown; observed reflections are those for which *h, k* and *l* are odd.

c) Inelastic scattering, soft modes and phase transitions

'Slow' neutrons possess kinetic energy that is comparable to the thermal energy levels in a solid. Such neutrons are inelastically scattered by phonons (i.e. vibrational modes) in the solid. From an analysis of the energy of the scattered neutrons, information on phonons and interatomic forces is obtained. For magnetic materials, further information on their electron exchange energy is obtained.

Displacive phase transitions are believed to be associated with the instability of a lattice vibration. A certain type of vibrational mode in the low temperature structure effectively collapses at the critical temperature. Such modes are called soft modes. They may be studied by IR and Raman spectroscopy, provided the vibrations involved are spectroscopically active, and also by neutron scattering. The latter technique is useful since it is not limited by the spectroscopic selection rules; by measuring the inelastic scattering about a number of 'Bragg reflections', the atomic displacements that are responsible for the soft mode and the phase transition may be determined. For instance, the mechanism of the displacive transition in quartz, SiO_2, at 573°C has been analysed by recording the neutron spectra at several temperatures below and above 573°C.